Electronic Supplementary Material (ESI) for Nanoscale.

Supplementary Information

Array of SiGe nanodisks with Ge quantum dots on bulk Si substrates demonstrating unique light-matter interaction associated with dual couplings

*Ningning Zhang, Shuguang Wang, Peizong Chen, Lijian Zhang, Kun Peng, Zuimin Jiang and Zhenyang Zhong**

State Key Laboratory of Surface Physics and Department of Physics, Fudan University, Shanghai 200438, People's Republic of China

*Corresponding author. E-mail:zhenyangz@fudan.edu.cn

S1. Experimental photoluminescence (PL) Setup of the incident laser and the PL collection

The Experimental PL Setup of the incident laser and the PL collection is schematically shown in Fig. S1. An Ar^+ laser (488 nm) is used for the excitation. The incident angle of the laser is ~50° (θ_1=~50°), and the ellipse laser spot on the sample surface has a size of R~1.5 mm. The PL is collected by a lens with a collection angle of 20° (θ_2=20°). Then it is focused by anther lens and passes through a slit to a monochromator (Omni-λ500, Zolix Instruments Co.) (not shown). The PL is finally detected

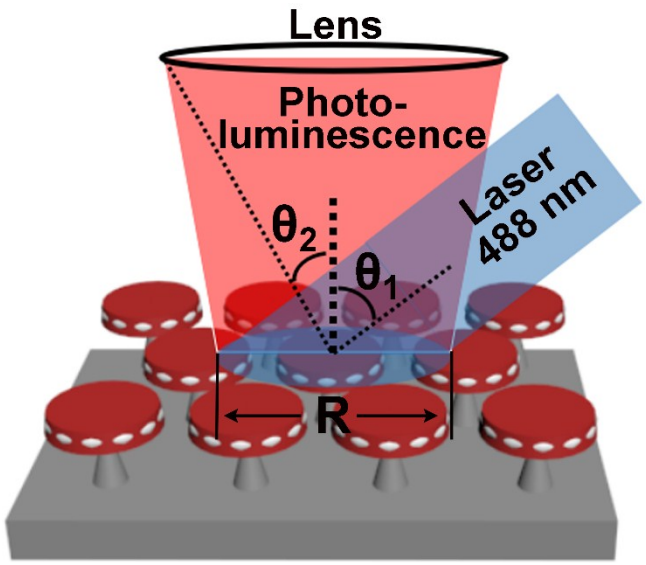

with an extended InGaAs photodetector using the standard lock-in technique.

Fig. S1. Schematic experimental Setup of the incidence of laser and the collection of PL.

S2. Surface morphology of Ge QDs

Fig. S2a shows the typical surface morphology after deposition of 8.2 monolayers (MLs) Ge at 520 °C on a 110nm thick $Si_{0.83}Ge_{0.17}$ alloy film on a miscut Si (001)/<110> 4° substrate. Self-assembled Ge QDs are readily obtained. Most of the Ge QDs are small and of asymmetrical pyramid-like shape. Their density is ~420/μm^2. Such small and dense QDs originate from the reduced activation energy for

the QD formation and reduced surface diffusion length of adatoms on the miscut substrates, which are consistent with the previous report.[1] Due to sufficient Ge deposition, some large dome-like QDs also appear.[2] Their density is ~21/μm^2. The height distribution of all Ge QDs is shown in Fig. S2b. It can be fitted by two Gaussian peaks, which clearly demonstrate two types of Ge QDs. The extracted average heights (±standard deviation) for the small and the large Ge QDs are 2.84 (±0.66) and 12.4 (±0.93) nm, respectively. The aspect ratio of the height over the lateral size for the small QDs is less than 0.1.

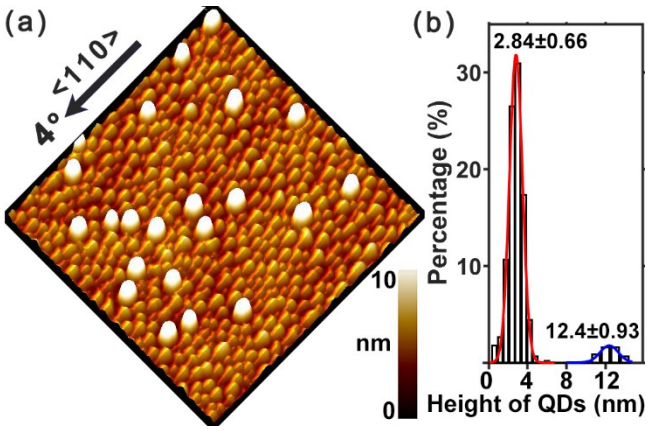

Fig. S2. Surface morphology of Ge QDs on a SiGe alloy film on a miscut Si (001)/<110> 4°substrate. (a) AFM image (1×1μm^2) of Ge QDs after 8.2 MLs Ge deposition at 520 °C on a 110 nm SiGe alloy film on a miscut Si (001)/<110> 4° substrate, (b) the height distribution of Ge QDs and the corresponding Gaussion fit.

S3. PL spectra from SiGe alloy films without and with Ge QDs, and from array of pillars

The normalized PL spectra of SiGe alloy film without Ge QDs and with Ge QDs, grown under the same growth conditions, are shown in Fig. S3a to clearly demonstrate the difference of the shapes and the wavelengths of peaks. It can be seen that the shapes and the wavelengths of two PL peaks (other than the peak from Si at 1128nm) are considerably different. For the sample of SiGe alloy film without Ge QDs, the peak around 1535nm naturally originates from SiGe alloy. However, for the sample of

SiGe alloy film with Ge QDs, the peak around the longer wavelength of 1625 nm essentially originates from Ge QDs since there is almost no distinguished peak around 1535 nm. In comparison with the SiGe alloy film, Ge QDs have smaller bandgap, which act as the efficient sink for the photon-generated carriers. Accordingly, most carriers around the SiGe alloy film are captured by the Ge QDs before their radiative recombination. Thus, the PL contribution from the SiGe alloy film can hardly be observed in case of the SiGe alloy film with embedded Ge QDs. Radiative recombination for some carriers in Si far away from Ge QDs and SiGe alloy can occur, which results in the peak at 1128 nm. It should be mentioned that the Ge composition in the SiGe alloy film is not ideally uniform under the present growth conditions. Some Ge-rich clusters appear in the SiGe alloy film, as shown in the high-resolution cross-sectional TEM image in Fig. S3b. The PL peak at 1535 nm is actually from those Ge-rich clusters in the SiGe alloy film. But the band gap of the Ge-rich clusters is still larger than that of the Ge QDs.

The PL spectrum of an array of pillars (SiGe alloy film with embedded Ge QDs on Si pillar) is shown in Fig. S3c, which is fabricated by the same processes but without the last step of selectively etching of Si in KOH solution for nanodisk array. The height of pillar is ~1 μm. The diameter and the periodicity of the pillars are nearly the same as those of nanodisks. In the range of concerned wavelengths from ~1350 nm to ~1900 nm, the shape and the intensity of the PL peak from SiGe alloy film with Ge QDs on the pillars are nearly the same as those from the unstructured substrate, as shown in Fig. S3c. Considering the small area of SiGe alloy film with Ge QDs on the pillars, the intensity of the PL peak from the unit area of SiGe alloy film with Ge QDs is slightly increased on the pillars due to the extraction of some PL from the sidewalls of pillars. But no remarkably strong peak at a particular wavelength is observed. This result clearly demonstrates that the observed PL enhancement in nanodisk array in the main text originates from Purcell effect instead of the light emission redistribution due to the presence of the vertical walls of disks.

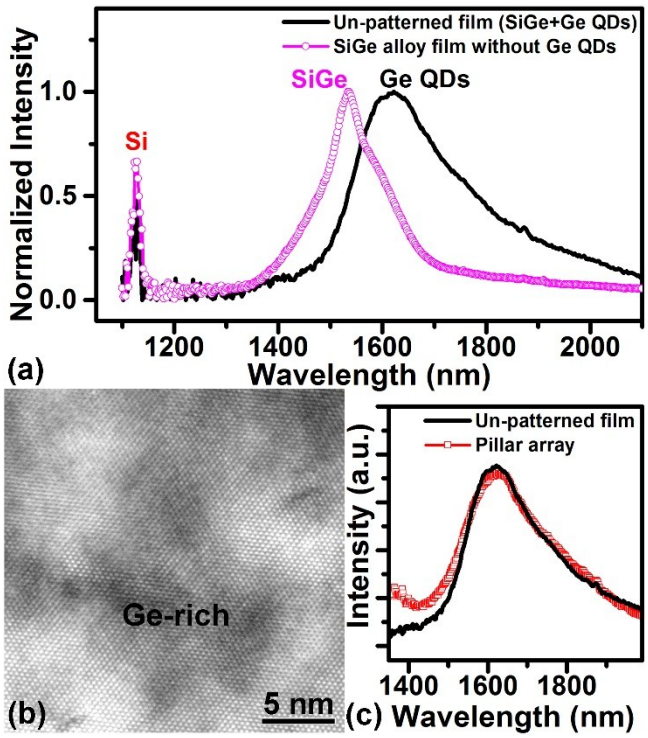

Fig. S3. (a) The normalized PL spectra of SiGe alloy film without Ge QDs and with Ge QDs, (b) the high-resolution cross-sectional TEM image of Ge-rich clusters in the SiGe alloy film; (c) the PL spectra of an array of pillars and un-patterned film of SiGe alloy with embedded Ge QDs on Si. The excitation power is 800 mW.

S4. Blue-shift of the PL peak of Ge QDs with the excitation power

The PL spectrum of Ge QDs in the un-patterned SiGe film can be decomposed into three Gaussian peaks with labels NP_S, NP_L and TO_L, as shown in the inset of Fig. S4. The dominant peak NP_S is attributed to the no-phonon (NP) emissions of the small and dense QDs.[1] The other two peaks NP_L and TO_L are assigned to be the NP emission and its transverse-optical (TO) phonon replica of the large QDs.[3] The wavelength of the dominant peak NP_S as a function of excitation power is shown in Fig. S4. Obviously, the dominant peak NP_S is blue-shifted with the excitation power. Similar blue-shifts occur for the peaks NP_L and TO_L (not shown). Such a blue-shift is typical for the type-II band alignment due to the band bending and/or band filling effects.[3]

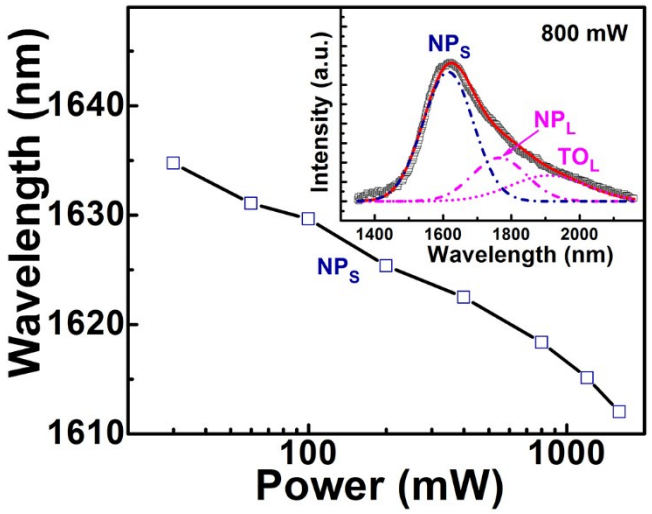

Fig. S4. Blue-shift of the PL peak of Ge QDs in the un-patterned SiGe alloy film with the excitation power. The wavelength of the dominant PL peak (NP_S) of Ge QDs in the un-patterned SiGe film as a function of the excitation power. The inset shows that the PL spectrum of Ge QDs can be decomposed into three Gaussian peaks with labels NP_S, NP_L and TO_L.

S5. The structure of nanodisk array used in FDTD simulations

The nanodisk array used in our FDTD simulations for models M2-4 is schematically shown in Fig. S5. A total of 91 nanodisks are considered in the simulations to avoid the effect of the boundary to the electromagnetic field distributions around the central nanodisk. The nanodisks are arranged in a two-dimensional hexagon lattice with the period of 1.1 μm. Perfectly matched layer (PML) boundary conditions are imposed. The distance between the boundary and the nanodisk array is 2 μm, as shown in Fig. S5. The geometrical profile of an individual nanodisk is schematically shown in the inset of Fig. S5, which is extracted from the SEM images. In order to simulate the emission spectrum of QDs embedded in the nanodisk, an electric dipole oriented along the x-axis is embedded in the middle plane of nanodisk, as denoted by a yellow arrow in the inset of Fig. S5. The electromagnetic field distributions around the central nanodisk are shown in Fig. 4 and 6 in the main text. They are essentially the same for the further increase of the involved nanodisks, as well as the simulated spectra.

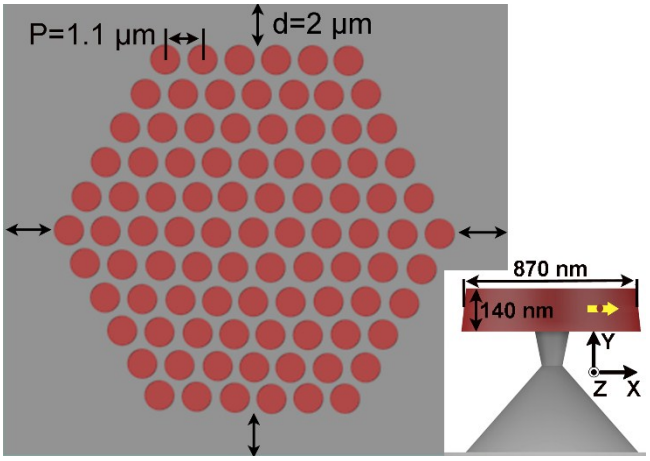

Fig. S5. The structure of nanodisk array used in FDTD simulations. A schematic nanodisk array in a two-dimensional hexagonal lattice with a period of 1.1 μm (denoted by P=1.1 μm). The distance between the PML boundary and the nanodisk array is 2 μm (denoted by d=2 μm). The individual nanodsik of 870 and 140 nm in diameter and thickness, respectively, is shown in the inset. The yellow arrow in the inset denotes an electric dipole embedded in the middle plane of nanodisk.

S6. Simulated spectra of nanodisk arrays with embedded dipoles of different orientation

The simulated spectra for x-, y- and z-oriented dipoles embedded at the same position in nanodisk arrays are shown in Fig. S6. The model M2 is used for the simulation, and the position of dipole is 120 nm away from the center of the nanodisk in the x direction. It is found that the simulated spectra for the y-oriented dipoles show the nearly same peak wavelengths as those for the x-oriented dipoles in the range of concerned wavelengths from ~1350 nm to ~1900 nm, except that the relative intensities are changed. The unique features discussed in the main text are essentially the same for x-oriented and y-oriented dipoles in the simulations. In addition, the z-oriented dipoles in nanodisks can also result in the nearly same resonant peaks but with significantly weak intensities.

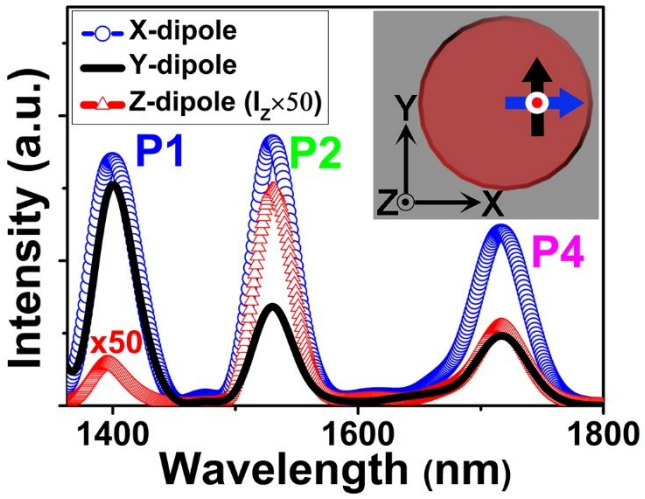

Fig. S6. The simulated spectra for x-, y- and z-oriented dipoles embedded at the same position in nanodisk arrays. The position of (x-, y- and z-oriented) dipole is 120 nm away from the center of the nanodisk in the x direction, as schematically shown in the inset. The spectrum for z-oriented dipole is multiplied by a factor of 50.

S7. Multipole decomposition of the anapole mode in a SiGe nanodisk

The multipole decomposition of the anapole mode in a SiGe nanodisk are demonstrated in Fig. S7, based on FDTD and decomposed discrete dipole approximation (DDDA) method.[4] For an isolated nanodisk shown in the inset of Fig. S7a, the contributions of a toroidal dipole and an electric dipole moments to the scattered field are equal at the wavelength of ~1680nm, as shown in Fig S7a. Accordingly, the completely destructive interference between the toroidal dipole and the electric dipole moments occurs, which result in an ideal anapole mode invisible at far field. In the case of a nanodisk supported by a pedestal on a substrate shown in the inset of Fig. S7b, the contributions of a toroidal dipole and an electric dipole moments to the scattered field are nearly the same around the wavelength of ~1700nm, as shown in Fig S7b. The slight difference is mainly due to the dissipation losses by the silicon pedestal.[5] Therefore, an incompletely destructive interference between the toroidal dipole and

the electric dipole moments occurs there, which give rise to an anapole mode with a weak and broad peak at far field.[4,5]

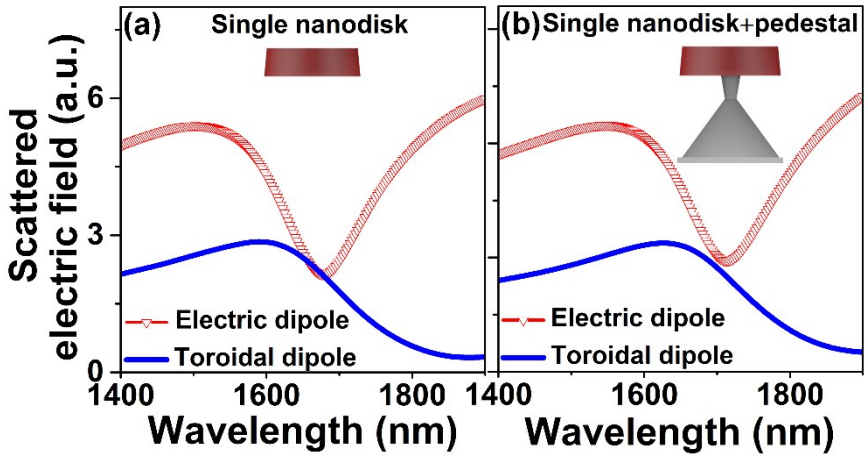

Fig. S7. The contributions of a toroidal dipole and an electric dipole moments to the scattered field as a function of wavelength (a) for an isolated nanodisk, (b) for a nanodisk supported by a pedestal on a substrate. The insets in (a) and (b) schematically show an isolated nanodisk and a nanodisk supported by a pedestal on a substrate, respectively. The diameter and the thickness of the SiGe nanodisk is 0.87 and 0.14 μm.

References

1 T. Zhou and Z. Zhong, *APL Materials*, 2014, **2**, 022108.

2 H. Yang, Z. Tao, J. Lin, F. Lu, Z. Jiang and Z. Zhong, *Applied Physics Letters*, 2008, **92**, 111907.

3 M. W. Dashiell, U. Denker and O. G. Schmidt, *Applied Physics Letters*, 2001, **79**, 2261-2263.

4 A. E. Miroshnichenko, A. B. Evlyukhin, Y. F. Yu, R. M. Bakker, A. Chipouline, A. I. Kuznetsov, B. Luk'yanchuk, B. N. Chichkov and Y. S. Kivshar, *Nature communications*, 2015, **6**, 8069.

5 A. A. Basharin, V. Chuguevsky, N. Volsky, M. Kafesaki and E. N. Economou, *Physical Review B*, 2017, **95**.